

Supporting Information

Enhancement of adsorption performance for organic molecules by combined effect of intermolecular interaction and morphology in porous rGO-incorporated hydrogels

*Seungmin Lee^{†,‡,1}, Byung Joon Moon^{†,1}, Hyun Jung Lee[§], Sukang Bae[†], Tae-Wook Kim[†],
Yong Chae Jung[†], Jong Hyeok Park[‡], and Sang Hyun Lee^{*,†}*

[†]Institute of Advanced Composite Materials, Korea Institute of Science and Technology, Chudong-ro 92, Bongdong-eup, Wanju-gun, Jeonbuk 55324, Republic of Korea.

[‡]Department of Chemical and Biomolecular Engineering, Yonsei University, 50 Yonsei-ro, Seodaemun-gu, Seoul 03722, Republic of Korea

[§]BioNano Health Guard Research Center, 125 Gwahak-ro, Yuseong-gu, Daejeon 34141, Republic of Korea

Corresponding Author (Dr. Lee)

E-mail address: sanghyun.lee@kist.re.kr

Table of Contents

1. Theoretical equations for adsorption
2. Visual dispersibility test for rGO sheets (**Figure S1**)
3. Photograph images of Ar-rGO composite aerogels (**Figures S2~S3**)
4. Cross-sectional SEM images of agarose and Ar-rGO₃₀ (**Figure S4**)
5. Composition ratios of Ar-rGO_x (**Table S1**)
6. Characterization of porous structure of the adsorbent (**Figures S5~S6 & Tables S2~S3**)
7. Static water contact angle analysis of Ar-rGO_x composites (**Figure S7**)
8. XPS analysis of agarose and rGO matrix (**Figures S8~S9**)
9. FT-IR, XPS and UV-vis absorption spectra of Ar and Ar-rGO₃₀ before/after adsorption of RhB (**Figures S10~S11**)
10. Kinetic study of RhB adsorption over agarose-based adsorbents (**Figures S12~S14 & Tables S4~S5**)
11. Adsorption isotherm study of the removal of RhB molecules (**Figure S15 & Tables S6~S7**)
12. Kinetic study of RhB desorption over Ar-rGO₃₀ (**Figures S16~S17**)
13. Effect of additives on the adsorption properties of adsorbents (**Figure S18**)
14. XPS and Raman analysis of rGO and GO (**Figure S19**)
15. Reusability and recyclability test of Ar-rGO₃₀ (**Figures S20~S22**)
16. pH-Stability test of Ar-rGOs at various pH values (**Figures S23~S24**)
17. Batch adsorption experiment for the removal of various organic pollutants (**Figure S25**)

1. Theoretical equations for adsorption

1.1 Adsorption kinetics.

(1) Pseudo-first-order kinetic model:

$$\ln(q_{e,cal} - q_t) = \ln q_{e,cal} - k_1 t \quad (1)$$

(2) Pseudo-second-order kinetic model:

$$\frac{t}{q_t} = \frac{1}{k_2 q_{e,cal}^2} + \frac{1}{q_e} t \quad (2)$$

where $q_{e,cal}$ is the calculated dye adsorption capacity (g/mg) at equilibrium. Also, k_1 (1/min) and k_2 (g/mg min) is the pseudo-first order rate constant of adsorption and the pseudo-second order rate constant of adsorption process, respectively.¹ Based on the slope and intercept of pseudo-first-order and pseudo-second-order model (Fig. 4c, d), the values of k_1 , k_2 and $q_{e,cal}$ were obtained as presented in Table S3. In addition, the validity of the kinetic models was evaluated in terms of regression coefficient (R^2).

(3) Intra-particle diffusion kinetic model:

$$q_t = k_{nd} t + C_n \quad (3)$$

where k_{nd} is the intra-particle diffusion constant (mg/g min^{1/2}) and C_n is the intercept at specific steps (n).²

1.2 Adsorption isotherms.

(1) Langmuir isotherm:

$$\frac{C_e}{q_e} = \frac{1}{q_m b} + \frac{C_e}{q_m} \quad (4)$$

where q_m is the maximum adsorption capacity (mg/g) of the adsorbent and b is the

Langmuir constant related to the energy of adsorption. Also, C_e is the concentration of adsorbate under equilibrium condition. The applicability of Langmuir equation depends upon the dimensionless factor R_L , which is calculated using the following equation:

$$R_L = \frac{1}{1 + bC_0} \quad (5)$$

where C_0 is the initial dye concentration (mg/L). The value of R_L between 0 and 1 supports favorable adsorption.

(2) Freundlich isotherm:

$$\log q_e = \log K_f + \frac{1}{n} \log C_e \quad (6)$$

where K_f and $1/n$ is the Freundlich constants related to adsorption capacity (L/g) and adsorption intensity.

(3) Dubinin-Kaganer-Radushkevich (DKR) isotherm:

$$\ln q_e = \ln q_D - \beta \varepsilon^2 \quad (7)$$

where q_D is the DKR isotherm constant related to degree of adsorption (mg/g), β is the activity coefficient and ε is the Polanyi potential, which is calculated using the following equation:

$$\varepsilon = RT \ln\left(1 + \frac{1}{C_e}\right) \quad (8)$$

Also, the apparent energy of adsorption (E) is calculated from the following equation:

$$E = \frac{1}{(2\beta)^{1/2}} \quad (9)$$

1.3 Thermodynamic parameters.

$$\Delta G^0 = -RT \ln K_L \quad (10)$$

$$\ln K_L = \frac{-\Delta H^0}{RT} + \frac{\Delta S^0}{R} \quad (11)$$

where R is the gas constant ($8.314 \text{ J mol}^{-1} \text{ K}^{-1}$), T is the absolute temperature in K , K_L is the distribution coefficient, ΔG^0 is the change in free energy, ΔS^0 is the change in entropy, ΔH^0 is the change in enthalpy.

2. Visual dispersibility test for rGO sheets

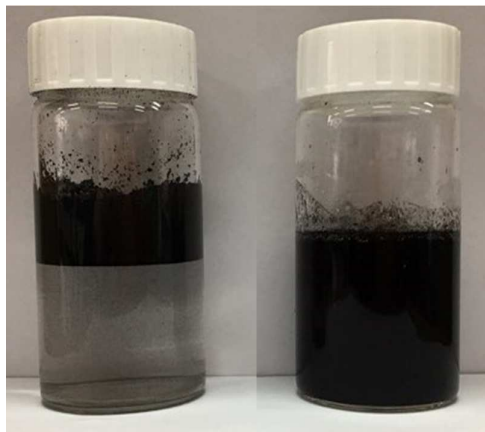


Figure S1. Visual dispersibility test for rGO (**Left:** only DI-water, **Right:** DI-water + agarose 2 wt%) at room temperature.

3. Photograph images of Ar-rGO composite aerogels

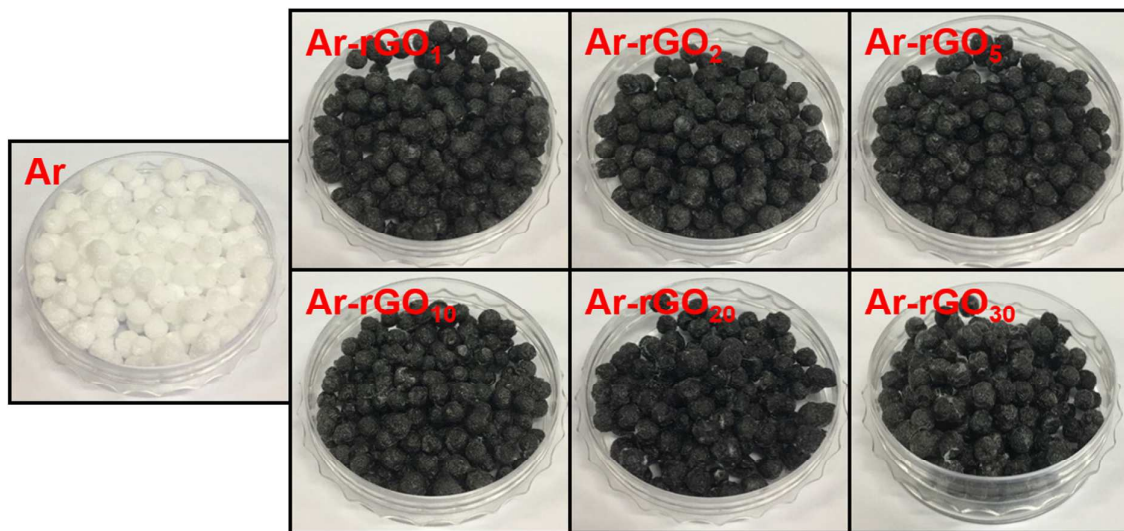


Figure S2. Optical photographs of Ar-rGO composites with different content of rGO.



Figure S3. Optical photographs of Ar-rGO composites in various forms. (cylinder, sphere, rectangle, and beads)

4. Cross-sectional SEM images of agarose and Ar-rGO₃₀

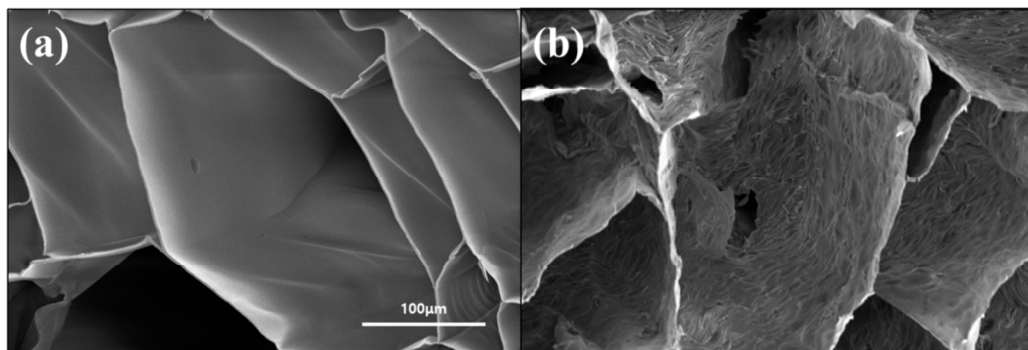


Figure S4. Cross-sectional FE-SEM images of (a) agarose and (b) Ar-rGO₃₀.

5. Composition ratios of Ar-rGO_x

Table S1. Composition ratios of Ar-rGO_x.

Sample	Agarose:rGO (weight ratio)	Agarose (weight, unit: g)	rGO (weight, unit: g)
Ar-rGO₂	98.0:2.0	0.2	0.004
Ar-rGO₅	95.2:4.8	0.2	0.01
Ar-rGO₁₀	90.9:9.1	0.2	0.02
Ar-rGO₂₀	83.3:16.7	0.2	0.04
Ar-rGO₃₀	76.9:23.1	0.2	0.06

6. Specific surface area, total pore area and average pore size of Ar-GO_x

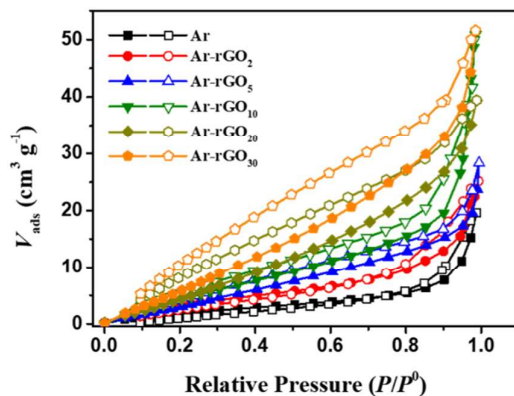


Figure S5. N₂ adsorption/desorption isotherms at 77 K of the adsorbents.

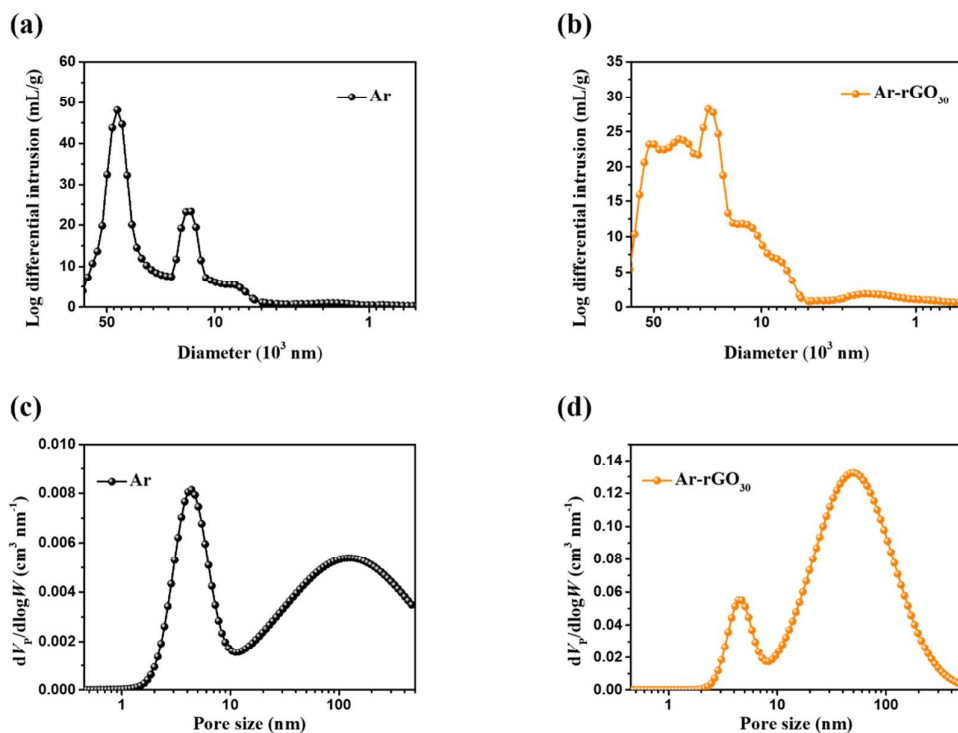


Figure S6. Macro-pore size distribution of the samples (Ar and Ar-rGO₃₀) obtained by mercury porosimetry (a, b). Micro- and mesopore volume distribution of the samples, analyzed by the NLDFT method (c, d).

Table S2. Specific surface area (SSA) of Ar and Ar-rGO_x.

Sample	Ar	Ar-rGO ₂	Ar-rGO ₅	Ar-rGO ₁₀	Ar-rGO ₂₀	Ar-rGO ₃₀
BET SSA (m ² /g)	8.296	13.950	17.789	23.457	28.976	35.629

Table S3. Pore volume and size of the adsorbents.

	BET SSA* (m ² /g)	Total pore volume* (cm ³ /g)	Mean pore Diameter* (nm)	Pore volume** (cm ³ /g)	Total pore area*** (m ² /g)	Average pore Diameter*** (μm)
Ar	8.296	0.0304	14.634	0.0395	33.765	2.185
Ar-rGO₃₀	35.629	0.0798	8.954	0.1345	60.402	1.431

* These values were calculated from BET method.

** These values were calculated from NLDFT method.

*** These parameters were examined by using mercury porosimetry.

7. Static water contact angle analysis of Ar-rGO_x composites

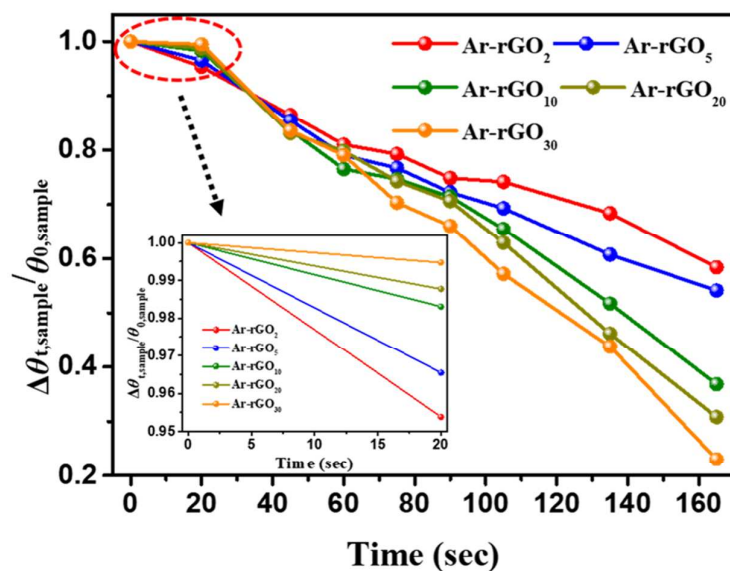


Figure S7. Relative contact angle variation of Ar-rGO_x composites, which can be triggered by water sorption into the samples, as function of retention time (Initial contact angle of water droplet: 75.17° (Ar-rGO₂), 79.38° (Ar-rGO₅), 82.16° (Ar-rGO₁₀), 84.06° (Ar-rGO₂₀) and 87.53° (Ar-rGO₃₀)).

8. XPS analysis of agarose and rGO matrixs

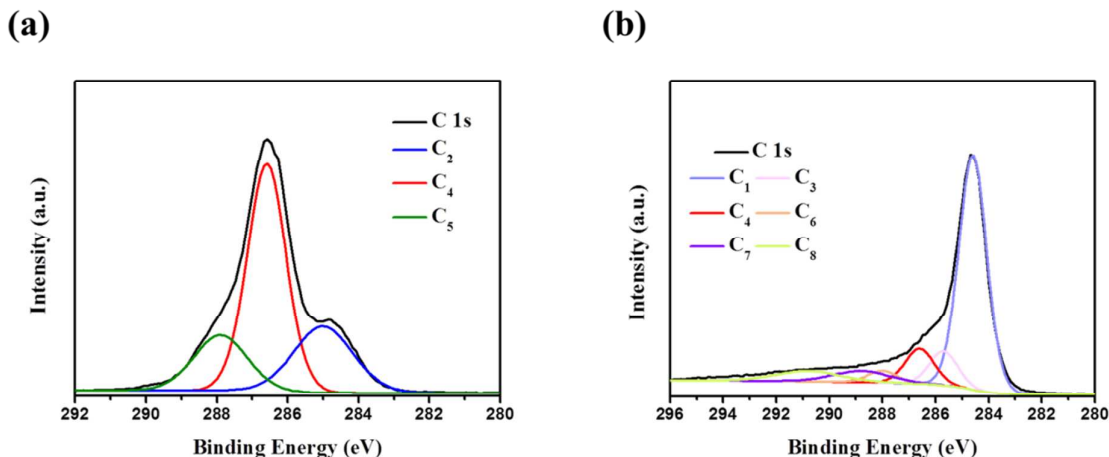


Figure S8. C 1s XPS spectra for (a) agarose and (b) rGO composites: The high-resolution C 1s spectrum of agarose can be deconvoluted into three signals for the C_xH_y structure (linear and saturated hydrocarbon, C_2), C-O bond (alkoxy group, C_4) and C-O-C bond (C_5) at 285.0, 286.6 and 287.9 eV, respectively, whereas that of rGO can be fitted to six components, including sp^2 C-C bond (C_1 , 284.6 eV), sp^3 C-C bond (C_3 , 285.7 eV), C_4 , C=O bond (carbonyl group, C_6 , 288.0 eV), O=C-O bond (carboxylic group, C_7 , 288.8 eV) and π - π^* satellite peak (C_8 , 290.8 eV).

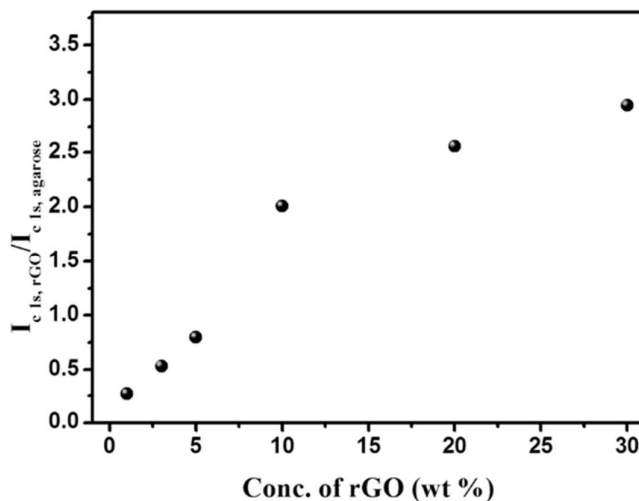


Figure S9. Relative peak-intensity ratio in C 1s spectra ($I_{C\ 1s,\ 284.6\ eV} / I_{C\ 1s,\ 286.6\ eV}$) as a function of rGO concentration in Ar-rGO_x.

9. FT-IR, XPS and UV-vis absorption spectra of Ar and Ar-rGO₃₀ before/after adsorption of RhB

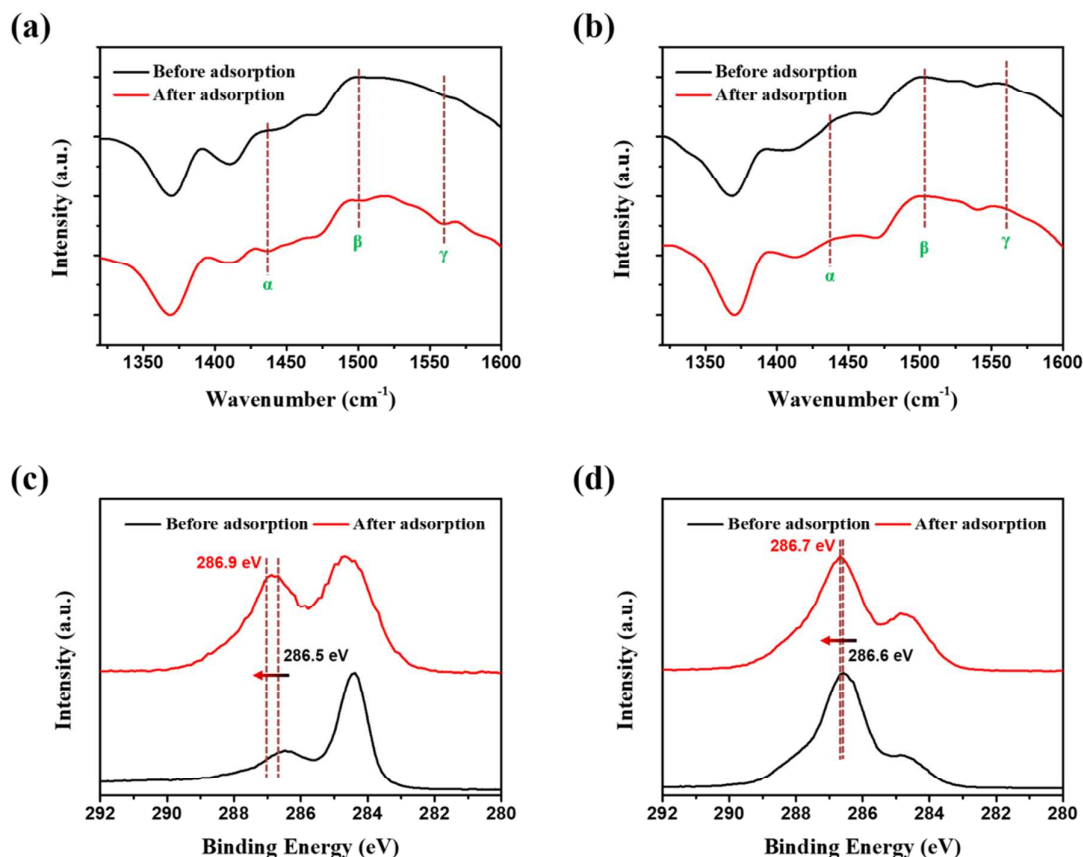


Figure S10. FT-IR spectra of (a) Ar-rGO₃₀ and (b) Ar (Peak assignments: approximately 1437 (symmetric stretching of non-hydrogen bonded C=O, denoted as α), 1503 (N–H stretching vibration, denoted as β) and 1575 (C=N, denoted as γ) cm⁻¹. The spectra were displayed within the wavelength of 1325~1600 cm⁻¹. C 1s spectra of (c) Ar-rGO₃₀ and (d) Ar (Peak assignments: C–O (approximately 286.5 eV) and C=O (approximately 287.0 eV). These adsorption experiments were performed under the following conditions: 500 mg/L (Initial Conc.); 1 mg/mL (adsorbent dose); 25 °C (temperature).

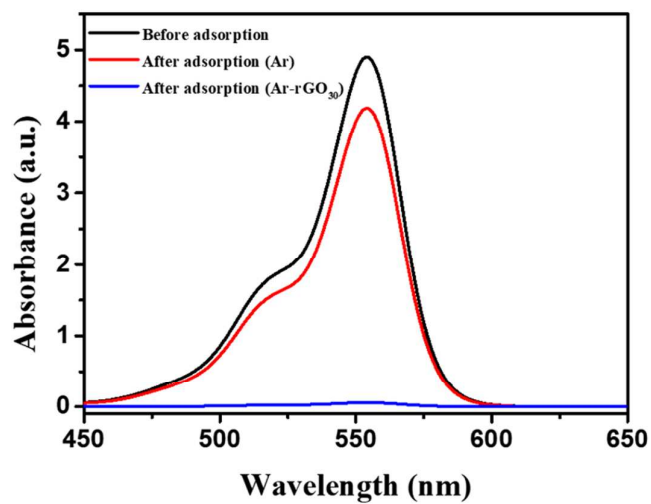


Figure S11. Representative UV-vis absorption spectra of RhB solution before and after the adsorption process (approximately 36 hr). These adsorption experiments were performed under the following conditions: 500 mg/L (Initial Conc.); 1 mg/mL (adsorbent dose); 25 °C (temperature); pH 7.0.

10. Kinetic study of RhB adsorption over agarose-based adsorbents

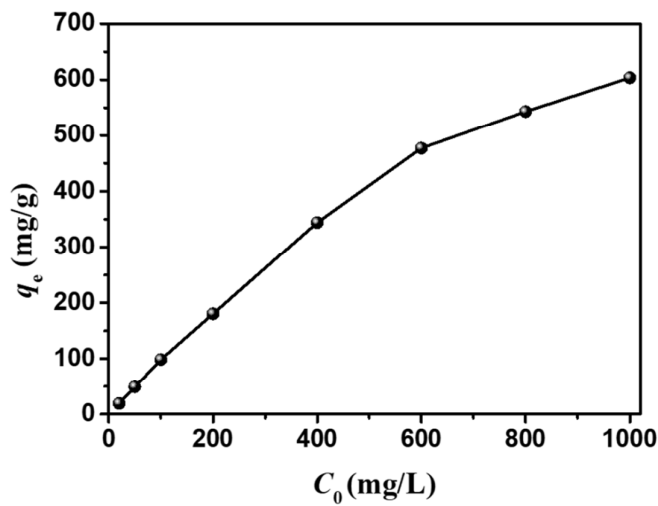


Figure S12. Effect of initial solution concentration (solvent: DI-water) on the adsorption capacity of RhB onto Ar-rGO₃₀. (adsorbent dose: 1 mg/mL and temperature: 25 °C)

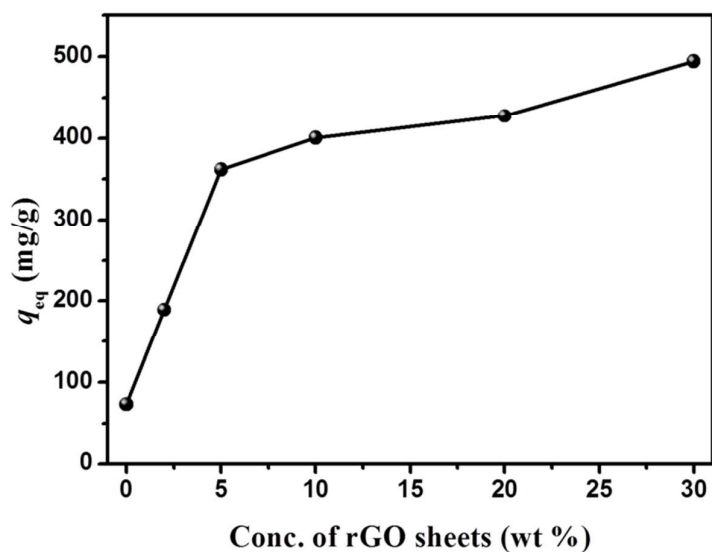


Figure S13. q_{eq} values of Ar-rGO_x as a function of rGO concentration. The absorbance of RhB at approximately 530 nm (λ_{max}) was used to determine the concentration of residual dye molecules for samples.

Table S4. Parameters of pseudo-first-order and pseudo-second-order kinetic models for the adsorption of RhB onto agarose and Ar-rGO_x.

	$q_{e,exp}$ (mg/g)	Pseudo-first-order model			Pseudo-second-order model		
		k_1 (10 ⁻³ /min)	$q_{e,cal}$ (mg/g)	R^2	k_2 (10 ⁻³ g/mg/min)	$q_{e,cal}$	R^2
Agarose	73.07	3.81	99.04	0.95874	8.78	113.90	0.77684
Ar-rGO₂	188.93	1.81	168.11	0.85958	4.81	207.90	0.97659
Ar-rGO₅	361.75	2.31	373.03	0.90299	2.42	413.22	0.98928
Ar-rGO₁₀	400.12	2.75	378.90	0.84081	2.32	431.04	0.99533
Ar-rGO₂₀	427.36	2.18	263.08	0.89288	2.22	450.45	0.99901
Ar-rGO₃₀	494.23	2.68	232.82	0.92930	1.95	512.82	0.99985

Table S5. Parameters of Intra-particle diffusion models for the adsorption of RhB onto agarose and Ar-rGO_x.

	Inter-particle Diffusion			
	k_{1d} (mg/g/min ^{1/2})	R^2	k_{2d} (mg/g/min ^{1/2})	R^2
Ar	0.71	0.94385	3.43	0.97709
Ar-rGO₃₀	24.80	0.98323	2.69	0.92327
Ar-rGO₃₀ (with agitation)	78.28	0.98403	10.72	0.93984

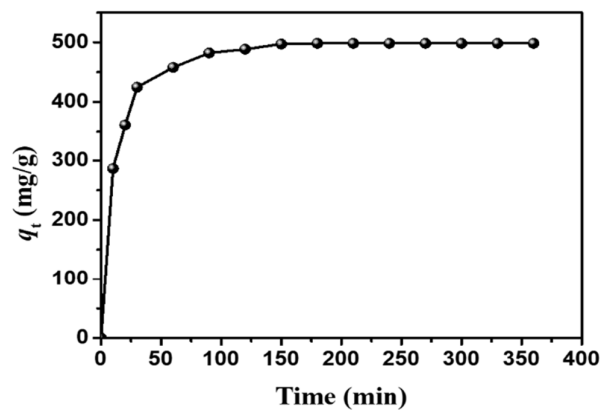


Figure S14. Effect of the agitation process on adsorption capacity of Ar-rGO₃₀ for RhB as function of adsorption time at room temperature. (Initial Conc.: 500 mg/L, adsorbent dose: 1 mg/mL, pH: 7.0 and temperature: 25 °C)

11. Adsorption isotherm study of the removal of RhB molecules

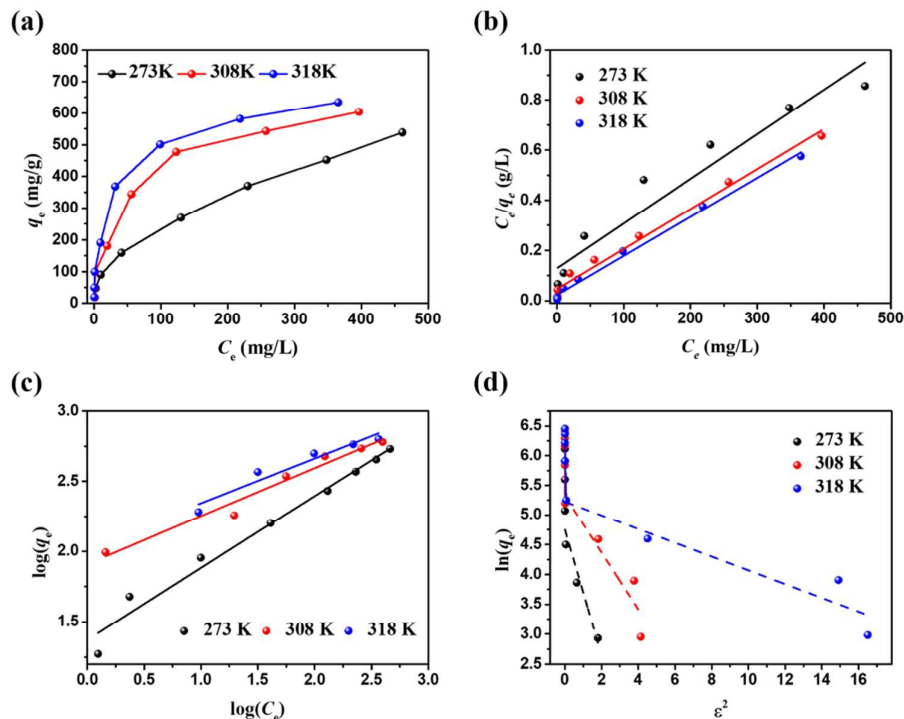


Figure S15. (a) Adsorption isotherms of RhB by the Ar-rGO₃₀ composite at different temperature. (b) Langmuir isotherms, (c) Freundlich isotherms and (d) DKR isotherms for the adsorption of RhB by the Ar-rGO₃₀ composite at different temperature. (Adsorbent dose: 1 mg/mL and pH: 7.0)

Table S6. Isotherm parameters for RhB adsorption onto Ar-rGO₃₀ composite.

Isotherms	Isotherm constants	Temperature (K)		
		273	308	318
Langmuir	q_m (mg/g)	561.80	628.93	645.16
	b (L/mg)	0.01379	0.03412	0.06641
	R^2	0.927	0.986	0.993
	R_L	0.0677 ~ 0.7838	0.0285 ~ 0.5944	0.0148 ~ 0.4295
Freundlich	$1/n$	2.2024	2.9222	3.1255
	K_F	31.3210	81.1947	105.3934
	R^2	0.997	0.964	0.923
Dubinin-Kaganer-Radushkevich (DKR)		Relatively low C_0		
	q_D (mg/g)	115.41	203.24	244.28
	E (KJ/mol)	0.6890	1.0261	2.0823
	R^2	0.886	0.825	0.847
		Relatively high C_0		
	q_D (mg/g)	413.81	506.79	529.22
	E (KJ/mol)	0.0389	0.0874	0.1828
	R^2	0.714	0.855	0.841

Table S7. Thermodynamic parameters for the adsorption of RhB onto Ar and Ar-rGO₃₀.

Sample	Temperature (°C)	Thermodynamic parameters		
		ΔG° (kJ/mol)	ΔH° (kJ/mol)	ΔS° (J/mol K)
Ar	273	5.88	6.43	2.03
	308			
	318			
Ar-rGO ₃₀	273	-6.41	6.07	45.71
	308	-7.23		
	318	-7.46		

12. Kinetic study of RhB desorption over Ar-rGO₃₀

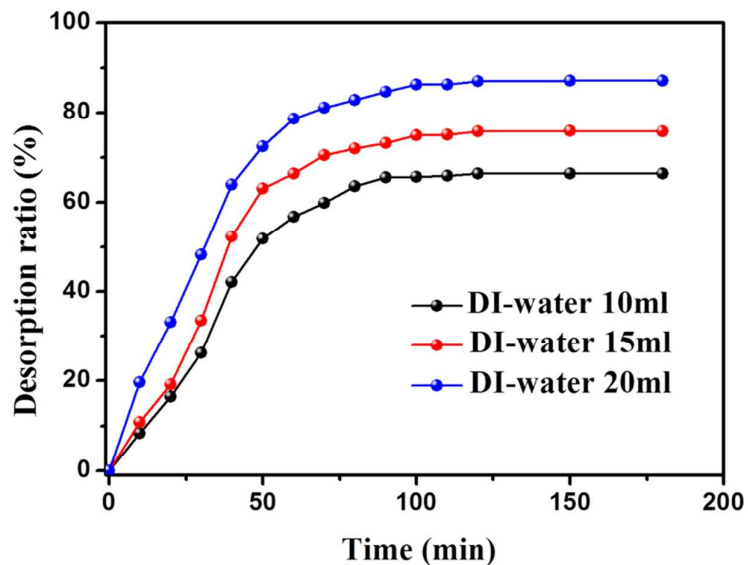


Figure S16. Desorption ratio of RhB molecules from Ar-rGO₃₀ beads over time. For this study, the adsorption experiment was performed under the following conditions: Initial Conc.: 500 mg/L, adsorbent dose: 1 mg/mL, pH: 7.0 and temperature: 25 °C.

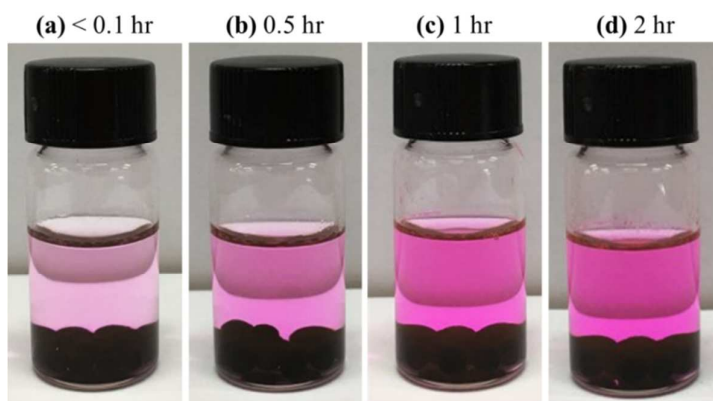


Figure S17. Optical photographs of Ar-rGO₃₀, which is adsorbed with RhB molecules, in DI-water for (a) less than 0.1 hr, (b) 0.5 hr, (c) 1 hr and (d) 2 hr.

13. Effect of additives on the adsorption properties of adsorbents

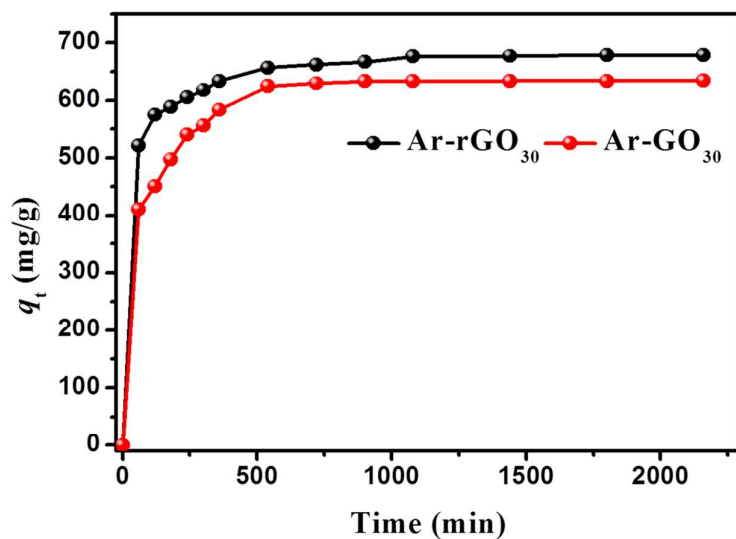
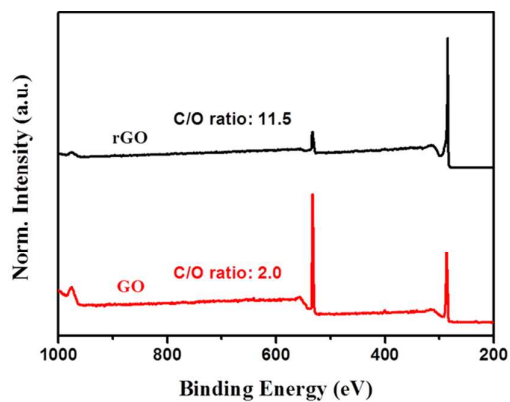


Figure S18. Effect of filler materials (GO and rGO) on adsorption capacity for RhB as function of adsorption time. (Initial Conc.: 750 mg/L, adsorbent dose: 1 mg/mL, pH: 7.0 and temperature: 25 °C)

14. XPS and Raman analysis of rGO and GO

(a)



(b)

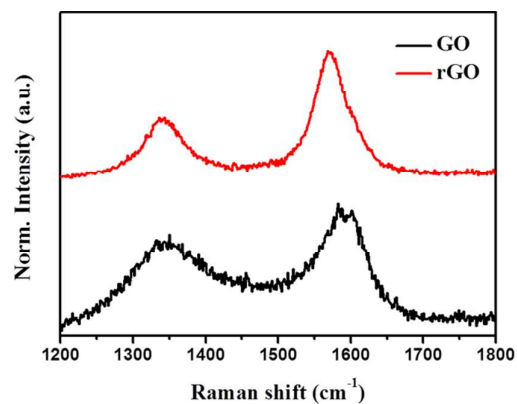


Figure S19. (a) Typical XPS survey spectra of rGO and GO. The focal X-ray beam size is approximately 200 μm . (b) Raman spectra of rGO and GO with green (514 nm) laser radiations.

15. Reusability and recyclability test of Ar-rGO₃₀

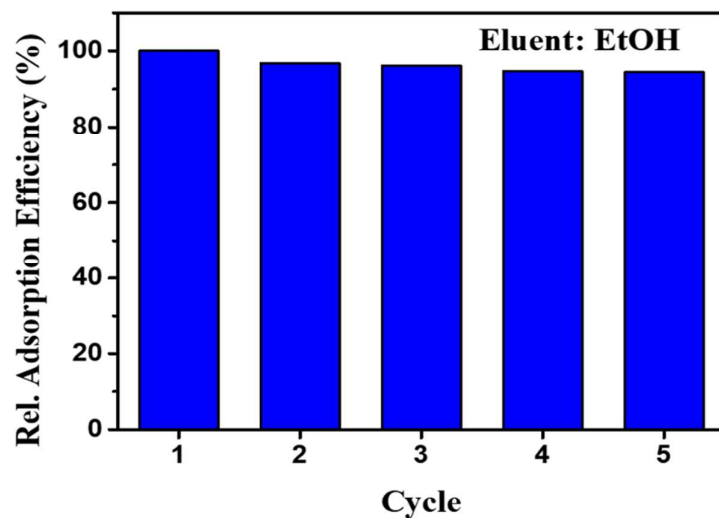


Figure S20. Recycling of Ar-rGO₃₀ composites for the capture of RhB molecules (Initial Conc.: 500 mg/L, Adsorbent dose: 1 mg/mL, Eluent Vol.: 10 mL and Temp.: 25 °C).

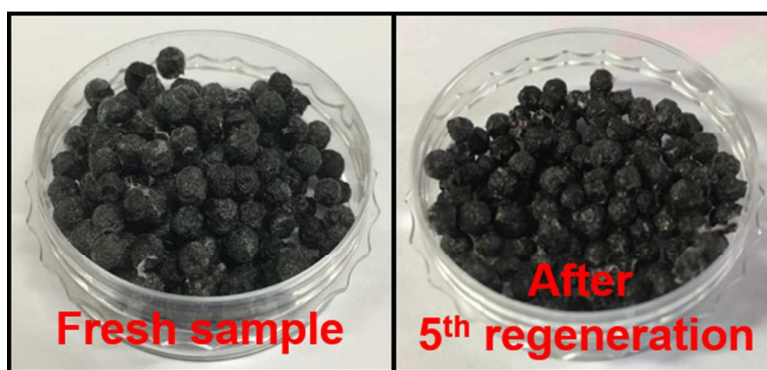


Figure S21. Optical photographs of Ar-rGO₃₀ beads (left: fresh sample & right: after 5th regeneration)

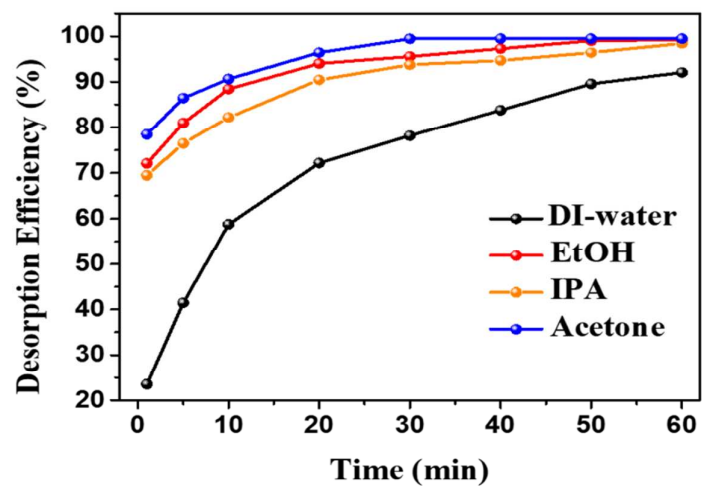


Figure S22. Desorption plots of RhB molecules by Ar-rGO₃₀. (Eluent Vol.: 30 mL, Temp.: 25 °C).

16. pH-Stability test of Ar-rGOs at various pH values

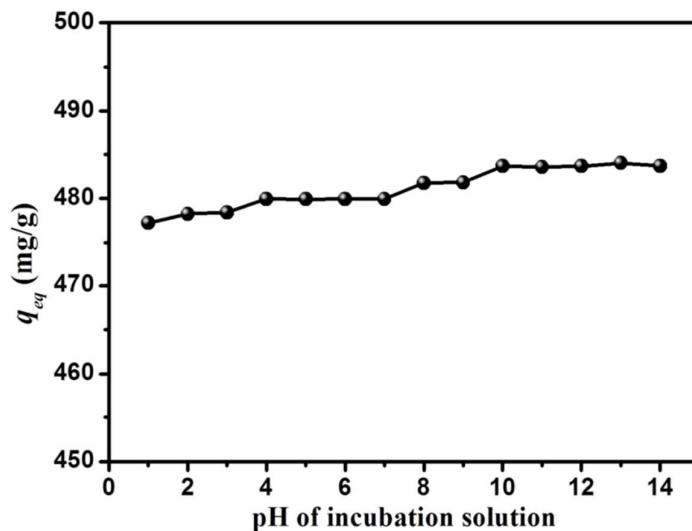


Figure S23. Effect of pH on stability of Ar-rGO₃₀. Ar-rGO₃₀ was incubated for 36 hr at room temperature (pH range: 1 ~ 14), thereafter it was washed with DI-water several times to get rid of the residual HCl or NaOH solution.

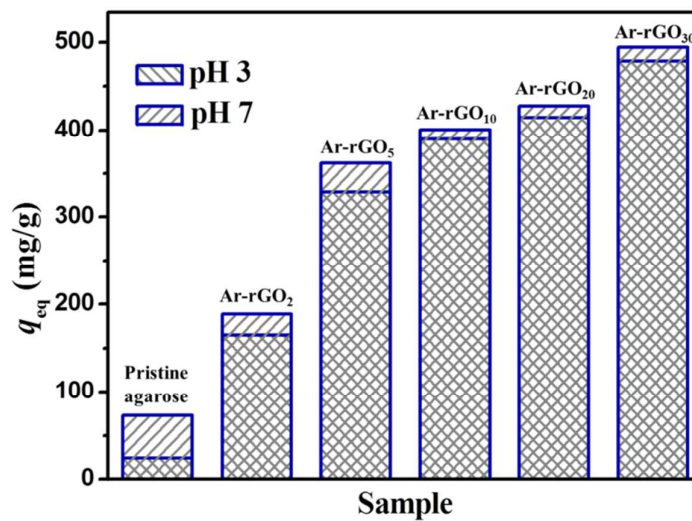


Figure S24. Effect of H⁺ ions on the adsorption performance of each adsorbent. (Initial Conc.: 500 mg/L, adsorbent dose: 1 mg/mL and temperature: 25 °C)

17. Batch adsorption experiment for the removal of various organic pollutants

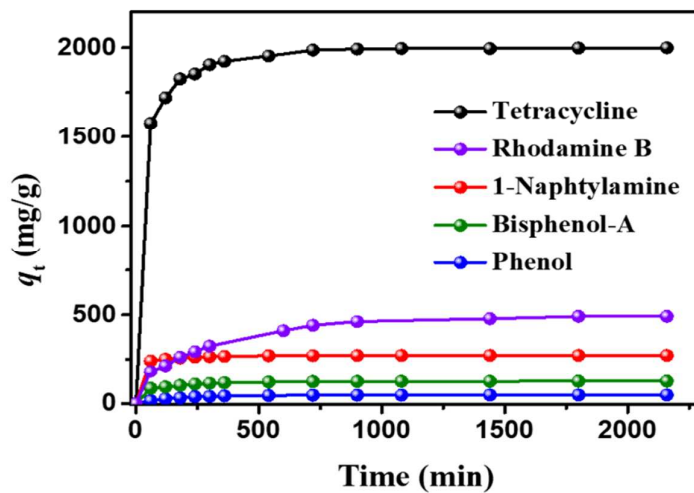


Figure S25. Kinetic data for the adsorption of various organic pollutants (Phenol, 1-Naphthylamine, Bisphenol-A, Rhodamine B and Tetracycline) by Ar-rGO₃₀. The initial concentration of solutions is 0.0005 mol/L.

REFERENCES

- (1) Azizian, S. Kinetic Models of Sorption: A Theoretical Analysis. *J. Colloid Interface Sci.* **2004**, 276, 47-52.
- (2) Furusawa, T.; Smith, J. M. Intraparticle Mass Transport in Slurries by Dynamic Adsorption Studies. *AIChE J.* **1974**, 20, 88-93.